Check for updates

Equivalent modeling and multi-parameter coupling optimization for DFIG-based wind farms considering SSO mode

Qian Zhang[1]*, Xuyang Jin[1], Fan Zhang[2], Hao Yuan[2] and Baorong Zhou[2]

[1]State Key Laboratory of Power Transmission Equipment and System Security and New Technology, Chongqing University, Chongqing, China, [2]State Key Laboratory of HVDC, Electric Power Research Institute CSG, Guangzhou, China

As a low-carbon and environmentally friendly renewable energy source, wind power has been globally recognized as the best solution to achieve energy saving and emission reduction and promote low-carbon economic growth. With the increase of wind power penetration, wind power has a great impact on sub-synchronous state stability and dynamic characteristics of the grid-connected system. Aiming at the fact that the correlation between clustering indexes and sub-synchronous oscillation (SSO) mode and the difference of the contribution to the clustering results are seldom considered in the current equivalent modeling of doubly-fed induction generator (DFIG)-based wind farm, this paper proposes a clustering method based on the index dimension reduction and weighted fuzzy C-means (WFCM) clustering algorithm. Besides, for the SSO study of the grid-connected system without sufficiently considering the coupling effects between controller parameters, a multi-parameter coupling optimization design strategy combining orthogonal experiment method (OEM) and response surface method is proposed. Firstly, the dominant variables of SSO mode of the DFIG-based wind farm connected to weak grid by series compensation system are taken as the initial clustering indexes. After dimension reduction by principal component analysis, the WFCM algorithm is utilized to cluster the wind farm. Then, the proportional and integral coefficients of the grid-side controller, rotor-side controller and phase-locked loop are optimized to achieve the simultaneous optimization of the SSO characteristics and dynamic characteristics of the system. Finally, the interaction between control parameters and the influence degree and trend on the system performance are quantitatively evaluated, and the optimal parameter combination is obtained. The proposed strategy can mitigate SSO more effectively while improving anti-interference than the particle swarm optimization based on OEM.

1 Introduction

Building a new power system with new energy as the main body and non-carbon energy as the carrier, and constructing a low-carbon and high-efficiency energy system are important ways to accelerate the construction of ecological civilization and realize the harmonious coexistence between human and nature (Huang et al., 2022). As a low-carbon and environmentally friendly renewable energy source, wind power has become an effective way to alleviate energy scarcity, combat climate change, and promote low-carbon economic growth worldwide (Xia et al., 2020). Doubly-fed induction generator (DFIG)-based wind farms are generally located in remote areas far from load centers. The strength of the grid is usually classified according to the short-circuit ratio (SCR). Generally, the grid with the value greater than 20 is considered as the strong grid and the value less than six is weak grid (Miao, 2012). As the grid-connected capacity of DFIGs continues to increase, the interaction between grid impedance and the equivalent impedance of DFIG-based wind farm can cause oscillations with weak grid operating condition. In addition, the series compensation capacitor will lead to the risk of sub-synchronous oscillation (SSO) (Liu et al., 2020; Leon et al., 2021). With the increasing penetration of wind power, equivalent modeling of wind farms has attracted attention at home and abroad. If each wind turbine is modeled in detail, it will not only increase the complexity of the power system model, but also be highly prone to the problem of dimensional disaster, which cannot reproduce SSO correctly (Han et al., 2020). Therefore, it is necessary to study dynamic equivalent modeling methods for wind farms to simplify the complexity of the model and reduce the computational effort.

Wind farm dynamic equivalence methods are generally divided into the single-machine equivalence method and the multi-machine equivalence method. The single-machine equivalence method equates all wind turbines into one unit, and the equivalent parameters are usually obtained by the weighted summation method (Pan et al., 2015). However, the actual operating conditions of the units within a large wind farm vary due to factors such as topography, wake effect, and time lag. When studying the dynamic characteristics of wind power grid-connected systems, the accuracy of the single-machine equivalence model cannot meet the actual demand. The multi-machine equivalence method clusters wind farms into multiple groups based on the principle that the operating conditions of wind turbines are the same or similar, and equates the wind turbine parameters of the same cluster, and finally uses several units to characterize the wind farm (Lei et al., 2013). The core idea of the multi-machine equivalence is to find

the attribute that characterizes the key features of DFIG and use this attribute for clustering. In (Shabanikia et al., 2021), a weighted dynamic aggregation method is proposed to obtain equivalent turbines for the problem of wind speed variations in different regions and different turbine parameters in wind farm aggregation modeling. A dynamic equivalence method for DFIG-based wind farms based on density-peak clustering algorithm is proposed in (Liu et al., 2019), which performs a two-stage clustering of wind farms based on the protection state of the crowbar and the transient characteristics of each unit under faults. In (Zhou et al., 2019), variables such as steady-state wind speed, slip rate, active power output, and rotor current are selected as indicators and Gaussian density distance clustering algorithm is used for clustering.

However, the current equivalence model does not consider the correlation between clustering indexes and SSO mode. It is inconclusive whether it is applicable to the analysis of SSO characteristics of DFIG-based wind farm connected to weak grid by series compensation systems. Moreover, the data set consisting of multiple DFIGs and clustering indexes may contain strongly correlated variables, making the effect of a particular index magnified and resulting in a bias in clustering results. Because of high dimensionality, the data is complicated and redundant, which leads to a long time spent in clustering. Most of the clustering algorithms currently used focus on the optimization of clustering centers and the determination of the number of clusters, ignoring the differences and correlations between clustering indexes.

The control system of DFIG consists of several PI controllers and the effects of different control parameters on the system performance vary greatly. The SSO can be effectively mitigated by reasonably adjusting control parameters to optimize the overall dynamic performance of the system. The main methods for optimizing DFIG control parameters are engineering tuning (Wanigasekara et al., 2022), small-signal analysis (Hu et al., 2022), and intelligent algorithm (Han et al., 2021). The engineering tuning relies too much on experience and there is "over-adjustment" or "blind adjustment" in the process of parameter adjustment; the small-signal analysis is not universal and is greatly influenced by the system operation state; the intelligent algorithm is difficult to obtain the optimization range and the global optimum cannot be satisfied. In (Bakir et al., 2020), the offline optimization of PI controllers at the rotor side of the DFIG wind energy system is achieved by bacterial foraging algorithm. In (Chen et al., 2019), based on participation factors and small signal model eigenvalues, the system damping is increased by exploring the optimal range of PI parameters. Most of the present studies on the optimization of DFIG parameters adopt intelligent

algorithms. There is a lack of analysis of the interaction between parameters, and it is easy to fall into local optimum due to the lack of clear optimization direction.

To address the above problems, the dominant variables of SSO mode of the DFIG-based wind farm connected to weak grid by series compensation system are taken as the initial clustering indexes. Considering the adaptation to dynamic and transient process analysis under multi-disturbance scenarios, a clustering method for DFIG-based wind farm based on the principal component analysis (PCA) and weighted fuzzy C-means (WFCM) clustering algorithm is proposed. The main contributions are as follows:

1) The proposed clustering method solves the problem that the correlation between clustering indexes and SSO mode, the contribution degree of different clustering indexes to the clustering results, and the inaccurate clustering caused by data redundancy are seldom considered in the equivalent modeling of the wind farm in the current study of the DFIG-based wind farm connected to weak grid by series compensation system.
2) A multi-parameter coupling optimization strategy combining orthogonal experiment method (OEM) and response surface method (RSM) is proposed to quantitatively analyze the interaction between each control parameter and the sensitivity and influence trend on the system performance, which solves the problem that the intelligent algorithm is easy to fall into local optimum.
3) Aiming at the simultaneous optimization of the sub-synchronous state stability and dynamic characteristics of the system, the control parameters of the clustered equivalent units are optimized. The optimal parameter combination is obtained, and the effective mitigation of SSO and the improvement of system anti-interference are achieved.

The rest of this paper is organized as follows: Section 2 introduces the DFIG-based wind farm clustering method based on the PCA and WFCM algorithm. The multi-parameter coupling optimization strategy based on the OEM-RSM is explained in Section 3. Section 4 gives the results of equivalence modeling and parameter optimization of the wind farm, and analyzes the interaction between control parameters and the influence degree on the performance of the grid-connected system. Conclusions and outlooks are drawn in Section 5.

2 Sub-synchronous oscillation equivalence of DFIG-based wind farm

2.1 Dimension reduction of clustering indexes based on PCA

2.1.1 Selection of clustering indexes for DFIG-based wind farm

In the DFIG-based wind farm connected to weak grid by series compensation system, the analysis of the SSO mechanism shows that the phase-locked loop (PLL) phase angle may affect the output voltages of grid-side controller (GSC) and rotor-side controller (RSC) and thus the output current of DFIG leading to system destabilization oscillation. And the fluctuation of DC-link voltage may affect the output current of DFIG and thus the grid voltage through GSC and RSC output voltages (Dong et al., 2016). Also, the grid strength, series compensation degree (SCD), DFIG d-axis and q-axis stator current and d-axis and q-axis rotor current are the main influencing factors of SSO (Liu et al., 2017). In order to better analyze SSO characteristics of the system, improve the effectiveness of clustering, and then design more targeted mitigation measures, this paper takes the dominant variables of SSO mode as clustering indexes: grid current angular frequency ω_s, DC-link voltage U_{dc}, d-axis stator current i_{sd}, q-axis stator current i_{sq}, d-axis rotor current i_{rd}, q-axis rotor i_{rq}.

The initial operating point of DFIG-based wind farm is an important basis for characterizing its steady-state properties. Different initial operating points affect the dynamic response of the wind turbine during SSO, resulting in differences in the state. Considering the adaptation to the analysis of dynamic and transient processes under multi-disturbance scenarios, this paper selects one time point of data before DFIG-based wind farm is connected to weak grid by series compensation (ω_{s1}, U_{dc1}, i_{sd1}, i_{sq1}, i_{rd1}, i_{rq1}), one time point of data during DFIG-based wind farm is connected to weak grid by series compensation (ω_{s2}, U_{dc2}, i_{sd2}, i_{sq2}, i_{rd2}, i_{rq2}), one time point of data during the fault (ω_{s3}, U_{dc3}, i_{sd3}, i_{sq3}, i_{rd3}, i_{rq3}), and one time point of data after fault removal (ω_{s4}, U_{dc4}, i_{sd4}, i_{sq4}, i_{rd4}, i_{rq4}). A total of 24 indexes are taken as initial clustering indexes.

2.1.2 Dimension reduction by PCA

The 24 initial clustering indexes may contain strongly correlated variables, which makes the weight and influence of a certain index magnified, resulting in a tendency of clustering results and affecting the accuracy of clustering. Moreover, the dimension of the data set is high and the data are complicated and redundant, so it takes longer time for clustering. Therefore, before using the initial clustering index to cluster DFIGs, it is necessary to process the data to eliminate the strong correlation and redundancy among them and reduce the negative impact on the clustering results caused by the interference of the data itself.

As a dimension reduction method for unsupervised learning, PCA is mainly used to reduce the dimension of dataset by measuring the amount of information through variance to eliminate the interaction between the original data (Sun et al., 2021). The magnitude of carrying the original feature variance information can be characterized by the contribution rate of principal component (PC). A larger contribution rate indicates that the PC is more capable of explaining the original feature information. In this paper, PCA is used to reduce the dimension of 24 initial clustering indexes in five steps (Li et al., 2019):

1) Build the sample matrix of the original data. The initial clustering index data extracted from the wind farm are constructed into a sample matrix X_w as shown in Eq. 1. Where n is the number of samples, i.e., the number of DFIGs in the wind farm; p is the number of indexes in each sample, and p is 24.

$$X_w = \begin{bmatrix} x_{11} & x_{12} & \cdots & x_{1p} \\ x_{21} & x_{22} & \cdots & x_{2p} \\ \vdots & \vdots & \ddots & \vdots \\ x_{n1} & x_{n2} & \cdots & x_{np} \end{bmatrix} = \begin{bmatrix} x_1, x_2, \ldots, x_p \end{bmatrix} \quad (1)$$

2) Calculate the sample covariance matrix. The data in X_w can be normalized by calculating the mean and standard deviation of the sample.

$$x_{ij}^* = \frac{x_{ij} - \overline{x_j}}{s_j^2} \ (i = 1, 2, \ldots, n, j = 1, 2, \ldots, p) \quad (2)$$

$$\overline{x}_j = \frac{1}{n} \sum_{i=1}^{n} x_{ij} \quad (3)$$

$$s_j^2 = \frac{1}{n-1} \sum_{i=1}^{n} \left(x_{ij} - \overline{x}_j \right)^2 \quad (4)$$

Where x_{ij} is the original sample data of the j-th index of the i-th DFIG; x_{ij}^* is the normalized data of x_{ij}; $\overline{x}_j$ and s_j^2 are the mean and standard deviation of the j-th index, respectively. X_w is normalized to X_w^* and the covariance matrix R_w can be obtained by Eq. 5. The correlation coefficient r_{ej} between x_e^* and x_j^* in X_w^* can be calculated from Eq. 6, where $\overline{x_e^*}$ and $\overline{x_j^*}$ are the mean values of the e-th and j-th indexes; x_{ie}^* and x_{ij}^* are the normalized data of the e-th and j-th indexes of the i-th DFIG, respectively.

$$R_w = \frac{1}{n} \left(X_w^* \right)^T X_w^* = \begin{bmatrix} r_{11} & r_{12} & \cdots & r_{1p} \\ r_{21} & r_{22} & \cdots & r_{2p} \\ \vdots & \vdots & \ddots & \vdots \\ r_{p1} & r_{p2} & \cdots & r_{pp} \end{bmatrix} \quad (5)$$

$$r_{ej} = \frac{\sum_{i=1}^{n} \left(x_{ie}^* - \overline{x_e^*} \right) \left(x_{ij}^* - \overline{x_j^*} \right)}{\sqrt{\sum_{i=1}^{n} \left(x_{ie}^* - \overline{x_e^*} \right)^2 \sum_{i=1}^{n} \left(x_{ij}^* - \overline{x_j^*} \right)^2}} \ (e, j = 1, 2, \ldots, p) \quad (6)$$

3) Calculate the eigenvalues of R_w and their corresponding eigenvectors. Establish the eigen equation $|\lambda I - R_w| = 0$ and apply the Jacobi method to solve it to obtain the eigenvalues. Arrange the eigenvalues in descending order to make $\lambda_1 \geq \lambda_2 \geq \cdots \geq \lambda_p \geq 0$. The corresponding eigenvectors can be obtained from the arranged eigenvalues as in Eq. 7, and then the eigenvector matrix V_w can be constructed.

$$\begin{cases} v_1 = \left(v_{11}, v_{21}, \cdots, v_{p1} \right)^T \\ v_2 = \left(v_{12}, v_{22}, \cdots, v_{p2} \right)^T \\ \vdots \\ v_p = \left(v_{1p}, v_{2p}, \cdots, v_{pp} \right)^T \end{cases} \quad (7)$$

4) Calculate the PC contribution rate and cumulative contribution rate.

$$\delta_j = \frac{\lambda_j}{\sum_{e=1}^{p} \lambda_e} \ (j = 1, 2, \ldots, p) \quad (8)$$

$$\mu_j = \frac{\sum_{j=1}^{j} \lambda_j}{\sum_{j=1}^{p} \lambda_j} \quad (9)$$

Where δ_j is the variance contribution rate of the j-th index; μ_j is the cumulative variance contribution rate of the first j indexes; λ_j is the eigenvalue of the j-th index. The variance contribution rate represents the ability to describe the original sample matrix. The larger the value is, the more information the original sample matrix contains, and the closer the reduced matrix is to the original matrix. The number of PCs is determined by cumulative contribution rate. To ensure the validity of data after dimension reduction and subsequent clustering, the first l PCs can reflect the information of p indexes when $\mu_l \geq 95\%$, so the first l PCs play the main role (Ma et al., 2021).

5) Construct the new sample matrix after dimension reduction. After determining the number of PC, take the first l rows of V_w to form a new matrix V_{wl}, and the new sample matrix after dimension reduction can be calculated as $Y_w = X_w^* V_{wl}$.

Compared with the initial data of DFIG-based wind farm, the reliability and validity of the data after dimension reduction by PCA are improved. Taking them as the clustering indexes of DFIG-based wind farm can improve the accuracy of clustering results.

2.2 Clustering of DFIG-based wind farm based on WFCM algorithm

2.2.1 WFCM clustering algorithm

FCM clustering algorithm is a method to describe and partition things with ambiguity or uncertainty (Zhao et al., 2022). When the traditional FCM algorithm is used to cluster wind turbines, the contribution degree of different clustering indexes to the clustering results is ignored, resulting in unreasonable clustering results. According to PCA, the contribution of each index is greatly different. Therefore, this paper proposes an FCM clustering algorithm with fixed weights of indexes by assigning corresponding weights to each index. The weights can be calculated by Eq. 10.

$$\begin{cases} PC = \dfrac{\lambda_1}{\lambda} PC_1 + \dfrac{\lambda_2}{\lambda} PC_2 + \cdots + \dfrac{\lambda_l}{\lambda} PC_l \\ \lambda = \lambda_1 + \lambda_2 + \cdots \lambda_l \\ \omega_k = \dfrac{\lambda_k}{\lambda} \ (k = 1, 2, \ldots, l) \end{cases} \quad (10)$$

Where PC_l is the l-th PC; λ_l is the eigenvalue of the l-th PC; ω_k is the weight of the k-th PC; and the weight vector of l PCs is $\boldsymbol{W} = \{\omega_1, \omega_2, \ldots, \omega_l\}$.

The reduced dimensional PC is taken as the clustering index of the DFIG-based wind farm. $\boldsymbol{Y}_w$ is the sample data set, where $y_i = \{y_{i1}, y_{i2}, \ldots, y_{il}\}$ is the i-th sample with l PCs. The WFCM algorithm can be calculated as follows:

1) Initialize the number of clusters $c\,(c \in [2, \sqrt{n}])$, the maximum number of iterations T_m, and the fuzzy index M. M is a constant that portrays the degree of fuzzification and takes a range of values from $[1, 2.5]$. Generally, M is 2 (Wang et al., 2020).
2) Determine the affiliation matrix $\boldsymbol{U}$ and the clustering center matrix $\boldsymbol{C}$. $\boldsymbol{U}$ is a matrix of $n \times c$, where u_{ih} is the affiliation of the i-th sample y_i in $\boldsymbol{Y}_w$ to the h-th clustering center, as shown in Eq. 11. $\boldsymbol{C}$ is a matrix of $c \times l$, where C_{hk} is given in Eq. 12.

$$u_{ih} = \dfrac{1}{\sum\limits_{m=1}^{c} \left(\dfrac{\sum\limits_{k=1}^{l} \omega_k \|y_{ik} - C_{hk}\|^2}{\sum\limits_{k=1}^{l} \omega_k \|y_{ik} - C_{mk}\|^2} \right)^{M-1}} \ (i = 1, 2, \ldots, n, h = 1, 2, \ldots, c)$$

$$(11)$$

$$C_{hk} = \dfrac{\sum\limits_{i=1}^{n} u_{ih}^{M} y_{ik}}{\sum\limits_{i=1}^{n} u_{ih}^{M}} \ (h = 1, 2, \ldots, c, k = 1, 2, \ldots, l) \quad (12)$$

Where y_{ik} is the i-th sample in $\boldsymbol{Y}_w$; $d^2(y_{ik}, C_{hk}) = \|y_{ik} - C_{hk}\|^2$ is the Euclidean distance from the i-th sample y_{ik} to the h-th clustering center.

3) Construct the objective function $F(\boldsymbol{U}, \boldsymbol{C}, \boldsymbol{W})$ as in Eq. 13 and the constraints as in Eq. 14.

$$\min F(\boldsymbol{U}, \boldsymbol{C}, \boldsymbol{W}) = \sum_{i=1}^{n} \sum_{h=1}^{c} \sum_{k=1}^{l} \left(u_{ih}^{M} \omega_k d^2(y_{ik}, C_{hk}) \right) \quad (13)$$

$$\begin{cases} 0 \leq u_{ih} \leq 1 \\ \sum\limits_{h=1}^{c} u_{ih} = 1 \\ \sum\limits_{k=1}^{l} \omega_k = 1 \end{cases} \quad (14)$$

4) Update the clustering center C_{hk} and the affiliation degree u_{ih} so that the objective function is the minimum, and keep repeating the above process until the number of iterations reaches T_m.

2.2.2 Clustering validity test

Clustering validity research is the process of evaluating the quality of clusters and determining the optimal number of clusters by establishing validity indexes (Chen et al., 2018). In order to ensure the accuracy and objectivity of the clustering results, the Xie-Beni(XB) index, which is widely used in fuzzy clustering, is chosen to determine the optimal number of clusters (Geng et al., 2019).

$$V_{XB} = \dfrac{\sum\limits_{i=1}^{n} \sum\limits_{h=1}^{c} \sum\limits_{k=1}^{l} \left(u_{ih}^{M} \omega_k d^2(C_{hk}, y_{ik}) \right)}{n \min\limits_{h \neq a} \sum\limits_{k=1}^{l} \left(\omega_k d^2(C_{hk}, C_{ak}) \right)} \ (a = 1, 2, \ldots, c) \quad (15)$$

The numerator of V_{XB} reflects the degree of compactness within a cluster, the smaller the value the more the compact; the denominator reflects the degree of separation between clusters, the larger the value the better the separation. Therefore, the smaller the value of V_{XB}, the better the clustering effect. The c corresponding to the smallest V_{XB} is the optimal clustering number.

To verify the rationality of the wind farm clustering indexes and further illustrate the effectiveness of WFCM algorithm and the rationality of clustering results, the Silhouette coefficient (SC) index and Calinski-Harabasz index (CHI) are selected for evaluation. The SC index is defined as follows:

$$SC_i = \dfrac{\beta_i - \alpha_i}{\max(\alpha_i, \beta_i)} \ (i = 1, 2, \ldots, n) \quad (16)$$

$$SC_m = \dfrac{1}{n} \sum_{i=1}^{n} SC_i \quad (17)$$

Where α_i is the intra-class compactness, which is the average distance between the sample y_i and all other samples in the same cluster, and the smaller the value, the more compact the cluster; β_i is the inter-class dispersion, which is the average distance between the sample y_i in any cluster and all samples in the nearest cluster, and the larger the value, the more disperse the cluster. SC_i is the profile coefficient of the i-th unit and $SC_i \in [-1, 1]$. $SC_i < 0$ indicates that the clustering is not reasonable, and the larger the value of SC_i, the more reasonable the clustering. SC_m is the average profile coefficient, and the larger the value, the more effective the clustering result.

The CHI takes into account the inter-class dispersion B and intra-class compactness W. Larger I_{CHI} indicates better inter-class dispersion and intra-class compactness. Where $\bar{y}$ is the mean value of all samples; $\varepsilon_{h,i}$ is the affiliation of the i-th sample to the h-th cluster.

$$I_{CHI} = \dfrac{B/(c-1)}{W/(n-c)} \quad (18)$$

$$\begin{cases} B = \sum\limits_{h=1}^{c} \sum\limits_{i=1}^{n} \varepsilon_{h,i} \|C_h - \bar{y}\|^2 \\ W = \sum\limits_{h=1}^{c} \sum\limits_{i=1}^{n} \varepsilon_{h,i} \|y_i - C_h\|^2 \\ \varepsilon_{h,i} = \begin{cases} 1, y_i \in C_h \\ 0, y_i \in C_h \end{cases} \end{cases} \quad (19)$$
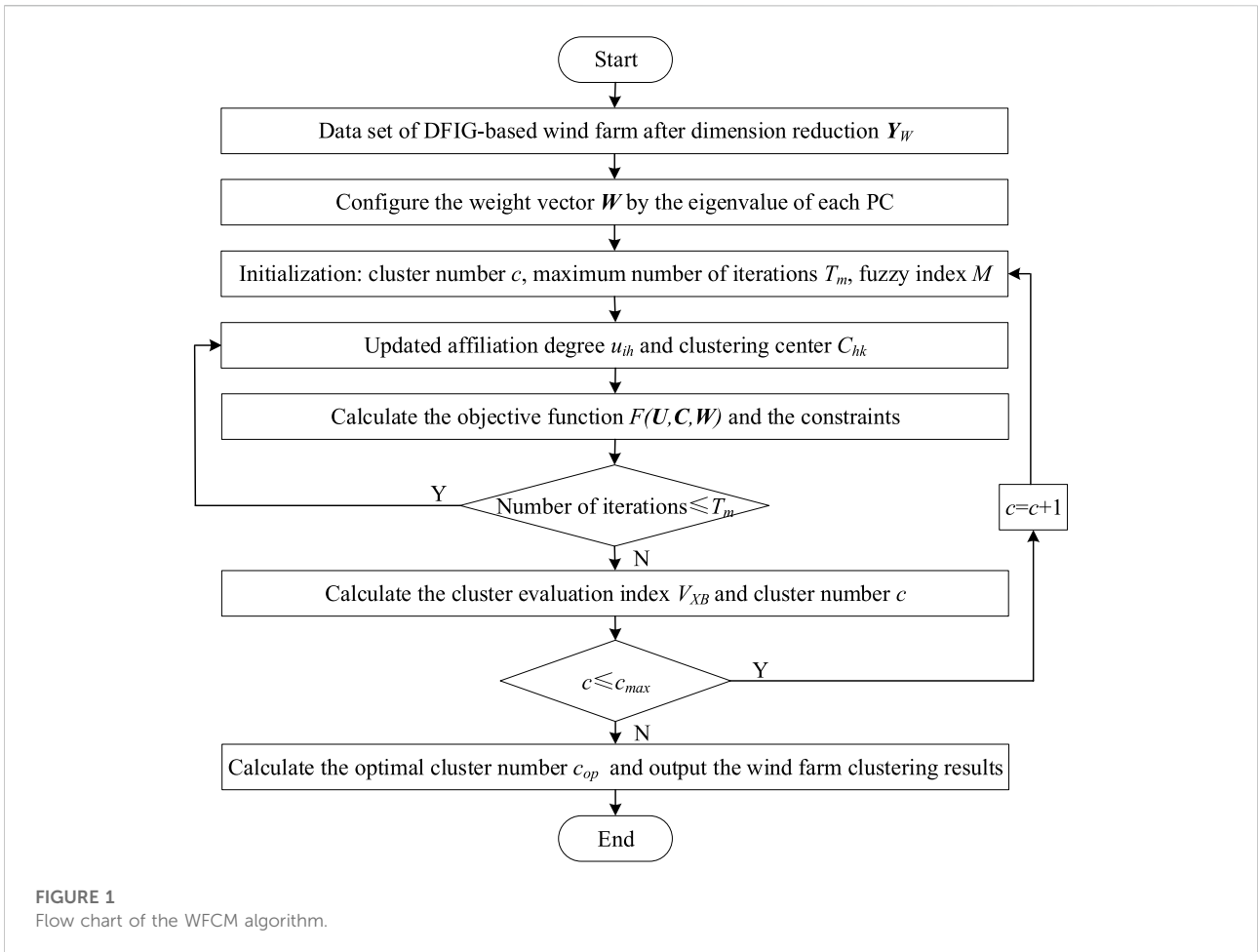
FIGURE 1
Flow chart of the WFCM algorithm.

The flow chart of the proposed WFCM algorithm is demonstrated in Figure 1.

2.3 Calculation of equivalent parameters for DFIG-based wind farm

According to the principle of constant output characteristics before and after equivalence, all the units in the cluster can be equivalent using the model of one unit. Assuming that there are d DFIGs of the same type in the same cluster after clustering by WFCM algorithm, the equivalent parameters can be calculated as follows:

$$
\begin{cases}
S_{eq} = \sum_{i=1}^{d} S_i, \, P_{eq} = \sum_{i=1}^{d} P_i, \, Q_{eq} = \sum_{i=1}^{d} Q_i \\[2mm]
H_{eq} = \sum_{i=1}^{d} H_i, \, D_{eq} = \sum_{i=1}^{d} D_i, \, K_{eq} = \sum_{i=1}^{d} K_i \\[2mm]
R_{eq} = \dfrac{R_s}{d}, X_{eq} = \dfrac{X_s}{d}, v_{eq} = \left(\dfrac{1}{d}\sum_{i=1}^{d} v_i^3\right)^{1/3}, \, Z_{Teq} = \dfrac{Z_T}{d}
\end{cases}
\tag{20}
$$

where the subscript eq is the equivalent parameter; the subscript i is the i-th wind turbine in the same cluster; $S, P, Q, H, D, K, R_s, X_s, v$, and Z_T are the rated capacity, active power, reactive power, inertia time constant, damping coefficient of shafting, stiffness coefficient of shafting, stator resistance, stator reactance, effective input wind speed, and transformer impedance, respectively.

According to the constant voltage difference before and after equivalent, the equivalent impedance of the trunk type collector line of the wind farm Z_{eq1} can be calculated by Eq. 21, and the equivalent impedance of the radial collector line Z_{eq2} can be calculated by Eq. 22. Where Z_f is the impedance of the f-th line; Z_i is the impedance of the i-th turbine line.

$$
Z_{eq1} = \frac{\sum_{i=1}^{d}\left(\sum_{f=1}^{i}\left(Z_f \sum_{b=f}^{n} P_b\right)P_i\right)}{\left(\sum_{i=1}^{d} P_i\right)^2}
\tag{21}
$$

$$
Z_{eq2} = \frac{\sum_{i=1}^{d} P_i^2 Z_i}{\left(\sum_{i=1}^{d} P_i\right)^2}
\tag{22}
$$

3 Multi-parameter coupling optimization design of DFIG-based wind farm based on OEM–RSM

In (Zhang et al., 2022), we have optimized the proportional and integral coefficients of GSC, RSC and PLL for a single DFIG connected to weak grid by series compensation system. Considering the SSO characteristics and dynamic characteristics of the system, the integrated average value of DC-link voltage overshoot ΔU_{dc}, active power overshoot ΔP_s, and grid current angular frequency overshoot $\Delta \omega_s$ when the disturbance occurs have been chosen as the performance indexes. After weighting by the analytic hierarchy process-coefficient of variation compound weighting method, the minimization of the weighted sum OD has been taken as the optimization objective. The control parameters have been optimized by OEM and particle swarm algorithm (PSO). As a result, the sensitivity and influence trend of control parameters on the system performance have been revealed, and the SSO has been effectively mitigated while ensuring strong anti-interference. However, the strategy is unable to analyze the interaction between parameters and is prone to fall into local optimum due to the use of intelligent algorithm. Therefore, this paper improves it and proposes a multi-parameter coupling optimization strategy for DFIG-based wind farms combining OEM and RSM.

The single-factor experiment method is to conduct experiments on only one factor while keeping all other factors constant, so as to explore the optimal range of values for each factor. The RSM uses a multiple quadratic regression equation to establish the functional relationship between the influencing factors and the response values based on the data obtained by the experimental design method, and the optimal parameter combination can be found by analyzing the equation (Si et al., 2018). It is generally utilized for experimental designs with few factors (generally 2–4) and few factor levels. In this paper, control parameters of each equivalent wind turbine are changed simultaneously and preliminary optimized by OEM to obtain the three factors that have the most significant influence on SSO and dynamic characteristics of the grid-connected system and seven insignificant factors. The seven insignificant factors can be valued according to the optimization results of OEM. Based on the values of three significant factors and the influence trend of them on OD, the single-factor experiment method is utilized to further determine the appropriate range of values. Set the values of each factor in RSM, a 3-factor, 3-level response surface experiment can be designed by Box-Behnken central combination. The experimental data of OD can be fitted according to the model with the best fit, and the model can be analyzed by analysis of variance (ANOVA) and constructed statistics. When all the indexes of the model meet the criteria, the regression equation between each factor and the evaluation index can be fitted, which can be expressed by Eq. 23. Then, the three-

dimensional response surface can be plotted to obtain the interaction between the factors and the optimal OD of the system and the corresponding levels of each factor.

$$y = c_0 + \sum_{i=1}^{N} c_i \xi_i + \sum_{i=1}^{N} c_{ii} \xi_i^2 + \sum_{i<j} \sum c_{ij} \xi_i \xi_j + \varepsilon, i, j = 1, 2, \cdots, N \tag{23}$$

Where ε is the fitting error, c_0 is a constant; c_i, c_{ii}, and c_{ij} are the coefficients of the first-order, second-order, and interaction terms, respectively; ξ_i and ξ_j are experiment factors.

4 Case study

4.1 Parameter setting

A time-domain simulation model of DFIG-based wind farm connected to weak grid by series compensation is built in Matlab/Simulink as shown in Figure 2. The wind farm contains 25 DFIGs of the same type, and the wind farm parameters and DFIG control parameters are shown in Table 1 and Table 2. The distance between each row of DFIGs is 500 m. The DFIG-based wind farm is connected to the 35 kV medium voltage bus through terminal transformers and overhead lines, and then the main

TABLE 1 Parameters of DFIG-based wind farm.

Parameters	Value
Base capacity S_B	0.8 MVA
Rated voltage U_B	690 V
Rated frequency f_B	50 Hz
Stator resistance R_s	0.03 p.u
Rotor resistance R_r	0.016 p.u
Stator leakage inductance L_{ls}	0.18 p.u
Rotor leakage inductance L_{lr}	0.16 p.u
Stator-rotor mutual inductance L_m	2.9 p.u
Grid-side filter inductance L_l	0.3 p.u
Grid-side filter inductance parasitic resistance R_l	0.02 p.u
DC-link capacitor C_{dc}	0.01 F
DC-link voltage U_{dc_ref}	1150 V
Terminal transformer rated capacity	1.67 MVA
Terminal transformer voltage ratio	0.69/35 kV
Terminal transformer X_T	6%
Main transformer rated capacity	50 MVA
Main transformer voltage ratio	35/220 kV
Main transformer X_T	10.5%
Line resistance R_L	0.115 Ω/km
Line inductance L_L	1.05e-3H/km
Line length	30 km
Distance between unit rows	0.5 km
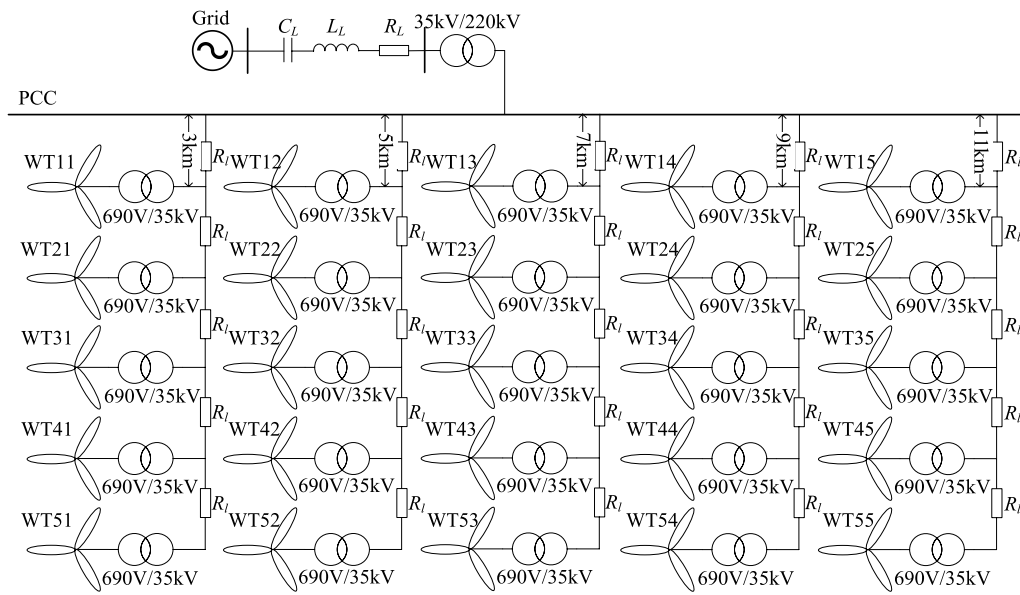
FIGURE 2
Topology structure of DFIG-based wind farm.

TABLE 2 DFIG control parameters.

Parameters	k_{p_dc}	k_{i_dc}	k_{p_il}	k_{i_il}	k_{p-p}
Value	6	400	0.8	5	1.6
Parameters	k_{i_p}	k_{p_ir}	k_{i_ir}	k_{p_pll}	k_{i_pll}
Value	100	0.6	8	5	1.1

TABLE 3 Wind speed of each unit in DFIG-based wind farm (m/s).

WT_{ij}	1	2	3	4	5
1	13.0000	13.0000	13.0000	13.0000	13.0000
2	13.0000	11.1719	11.1719	11.1719	13.0000
3	11.1719	11.1719	9.3866	9.3866	13.0000
4	9.3866	11.1719	9.3866	7.9655	13.0000
5	7.9655	11.1719	9.3866	7.9655	7.1540

transformer is connected to the 220 kV grid through the transmission line. According to the wind speed, wind direction, and wake effect, the wind speed of each unit in the wind farm can be calculated as shown in Table 3.

4.2 Equivalent modeling results for DFIG-based wind farm

The initial SCR is set to 3 and SCD is 20%. The SCR is changed to 2 and SCD is changed to 60% at 2.1 s. The SCR and SCD are changed back to initial values at 3.1 s. A three-phase ground short-circuit fault is occurred at 4 s and removed at 4.15 s. The data collected at 2s are $\omega_{s1}, U_{dc1}, i_{sd1}, i_{sq1}, i_{rd1}, i_{rq1}$, the data collected at 3 s are $\omega_{s2}, U_{dc2}, i_{sd2}, i_{sq2}, i_{rd2}, i_{rq2}$, the data collected at 4.1s are $\omega_{s3}, U_{dc3}, i_{sd3}, i_{sq3}, i_{rd3}, i_{rq3}$, and the data collected at 4.6s are $\omega_{s4}, U_{dc4}, i_{sd4}, i_{sq4}, i_{rd4}, i_{rq4}$. The data set consisting of 25 DFIGs and 24 initial clustering indexes is the sample matrix X_w of 25×24.

4.2.1 Results of dimension reduction by PCA

The dimension of X_w is reduced by PCA. The eigenvalues of each component are arranged in descending order, and the corresponding variance contribution rate and cumulative contribution rate are calculated as shown in Table 4.

It can be found that the 24 initial clustering indexes contain strongly correlated indexes, which will cause bias in the clustering results, so the dimension of data need to be reduced. The cumulative contribution rate of the first three PCs has reached 96.7319%, greater than 95%, which meets the requirement for the selection of PCs in PCA, while the remaining indexes have little influence on contribution. The contribution rates of the first three PCs are 51.4265%, 33.9819%, and 11.3236%, respectively. Therefore, the first three PCs can be selected for dimension reduction, i.e., the initial clustering indexes are reduced to 3 dimensions. The component with the eigenvalue of 12.34236 is the first PC, the component with the eigenvalue of

TABLE 4 Contribution rates of PCs.

PC	Eigenvalue	Variance contribution rate	Cumulative contribution rate	PC	Eigenvalue	Variance contribution rate	Cumulative contribution rate
1	12.34236	0.514265	0.514265	13	2.79E-06	1.16E-07	1
2	8.155651	0.339819	0.854084	14	1.11E-06	4.63E-08	1
3	2.717655	0.113236	0.967319	15	2.33E-07	9.71E-09	1
4	0.567313	0.023638	0.990957	16	6.1E-08	2.54E-09	1
5	0.157528	0.006564	0.997521	17	8.24E-09	3.43E-10	1
6	0.040513	0.001688	0.999209	18	6.79E-10	2.83E-11	1
7	0.015618	0.000651	0.99986	19	3.16E-11	1.32E-12	1
8	0.002584	0.000108	0.999967	20	8.03E-12	3.34E-13	1
9	0.000376	1.57E-05	0.999983	21	1.56E-13	6.52E-15	1
10	0.000266	1.11E-05	0.999994	22	1.57E-14	6.51E-16	1
11	9.14E-05	3.81E-06	0.999998	23	4.85E-15	2.05E-16	1
12	4.52E-05	1.88E-06	1	24	-1.6E-16	-6.8E-18	1

FIGURE 3
Contribution rates of PCs.

(15), the optimal cluster for 25 DFIGs $c_{op} = 4$. Thus the clustering results with 3 PCs as multiple clustering indexes can be obtained in Table 5; Figure 4.

In order to verify the effectiveness of WFCM algorithm and the reasonableness of clustering results, Figure 5A shows the profile coefficients of 25 DFIGs when the clusters is 4, Figure 5B shows the results of average profile coefficient, and Figure 5C shows the results of CHI.

It can be observed from Figure 5A that the profile coefficients of 25 DFIGs are all greater than 0 when the cluster is 4, indicating the clustering is reasonable and effective. From Figure 5B,C, the average profile coefficient and CHI are both maximum at the cluster of 4, which is consistent with XB index. Therefore, the 25 DFIGs built in this paper can be divided into four equivalent clusters.

4.3 Multi-parameter coupling optimization results for DFIG-based wind farm

The equivalent wind farm after clustering are preliminarily optimized by OEM, and the values of each control parameter can be obtained as shown in Table 6. From the results of OEM, the three factors that have the most significant effect on SSO characteristics and dynamic characteristics of DFIG-based wind farm connected to weak grid by series compensation system are GSC DC voltage loop proportional coefficient k_{p_dc}, RSC current loop proportional coefficient k_{p_ir}, and PLL proportional coefficient k_{p_pll}. And the optimized values are 10, 0.5, and 3, respectively. The single-factor experiments are conducted for these three factors to narrow their range of values. The corresponding generalized Nyquist curves of the system scaled up at $(-1, j0)$ are drawn in Figure 6.
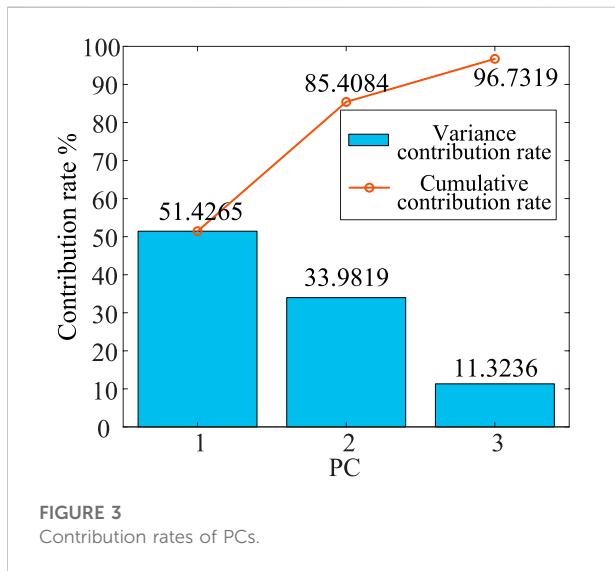
8.155651 is the second PC, and the component with the eigenvalue of 2.717655 is the third PC, which basically retains the information of the original data. The contribution rates of these three PCs are given in Figure 3.

So far, the dimension of 24 initial clustering indexes are reduced to obtain 3 PC indexes by PCA, and the new sample matrix after dimension reduction Y_w is of 25×3. The weight vector of the 3 PCs can be calculated as $W = \{0.5316, 0.3513, 0.1171\}$ according to (10).

4.2.2 Clustering results for DFIG-based wind farm

Y_w is clustered by WFCM clustering algorithm. c is set as 2, T_m is set as 100, and M is set as 2. According to the iteration of

TABLE 5 The clustering results for DFIG-based wind farm by WFCM.

Cluster	Clustering results
1	WT_{14}, WT_{24}, WT_{15}, WT_{25}, WT_{35}, WT_{45}
2	WT_{44}, WT_{54}, WT_{55}
3	WT_{41}, WT_{51}, WT_{33}, WT_{43}, WT_{53}, WT_{34}
4	WT_{11}, WT_{21}, WT_{31}, WT_{12}, WT_{22}, WT_{32}, WT_{42}, WT_{52}, WT_{13}, WT_{23}

TABLE 6 Optimal parameter combination based on OEM.

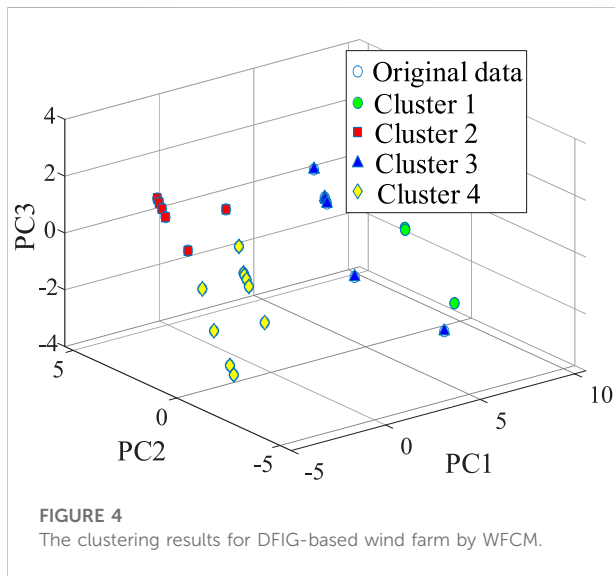| Parameters	k_{p_dc}	k_{i_dc}	k_{p_il}	k_{i_il}	k_{p_p}
Value	10	380	0.6	5	1.6
Parameters	k_{i_p}	k_{p_ir}	k_{i_ir}	k_{p_pll}	k_{i_pll}
Value	100	0.5	8	3	0.8

FIGURE 4
The clustering results for DFIG-based wind farm by WFCM.

According to the generalized Nyquist stability criterion, if the Nyquist curves do not enclose (−1, j0), the system is stable and the further away from that point, the more stable the system is. It can be found that the optimal value exists between 45 and 55 for k_{p_dc}, 0.45 to 0.55 for k_{p_ir}, and 2 to 3 for k_{p_pll}. And the Nyquist

curves do not enclose (−1, j0) within the above values, indicating that the system is stable. So the value ranges of each parameter determined by the single-factor experiment method is reasonable and valid. The response surface experiment is designed in Design-Expert 11, and the level values of k_{p_dc} are set as 45, 50, and 55, the level values of k_{p_ir} are 0.45, 0.5, and 0.55, and the level values of k_{p_pll} are 2, 2.5, and 3. A total of 17 sets of experiments are conducted. A quadratic polynomial model is fitted to the experimental data of *OD*, and the results of ANOVA on the model are shown in Table 7. The constructed statistics are shown in Table 8.

As can be seen from Table 7, the *p*-value of the model is less than 0.0001, indicating that the overall effect of the parameter combination on *OD* is extremely significant. Linear terms A, B and quadratic term B^2 have an extremely significant effect on *OD*, quadratic term C^2 has a highly significant effect on *OD*, interaction term BC has a significant effect on *OD*, and the effects of other terms are not significant. The significance of the effect of each factor is A > B > C, that is, $k_{p\_dc} > k_{p\_ir} > k_{p\_pll}$. The *p*-value of the lack of fit in the table is greater than 0.05 (0.2951), indicating that the lack of fit is not significant, so the model is able to fit the data accurately.

The statistics of the experiment data should meet the requirements of C.V.% less than 10, precision greater than 4, R^2, adjusted R^2, and predicted R^2 are close to 0.9, and the
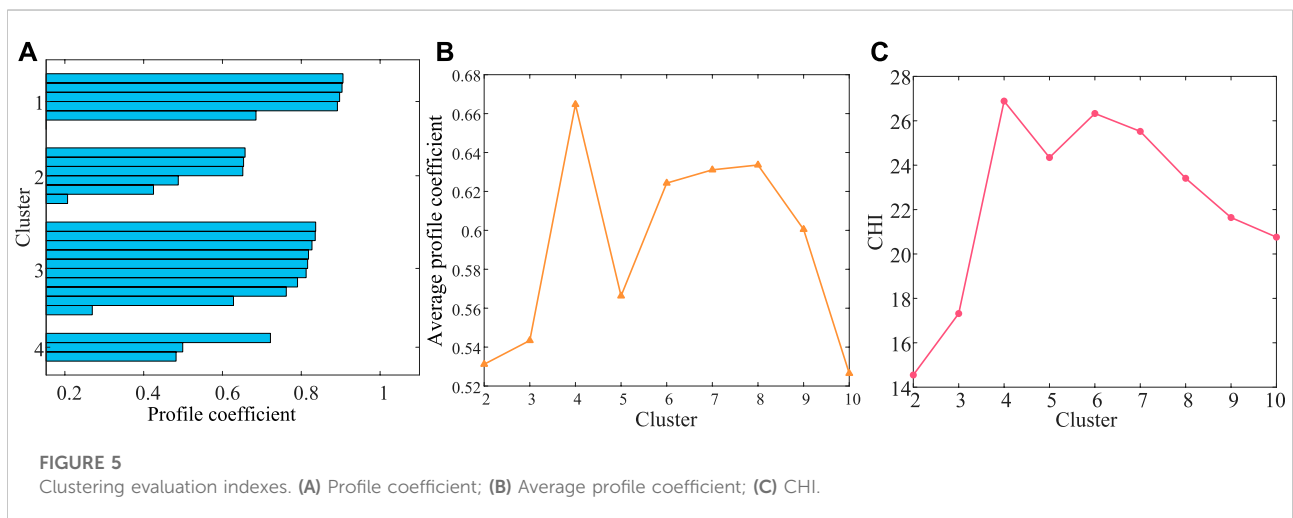

FIGURE 5
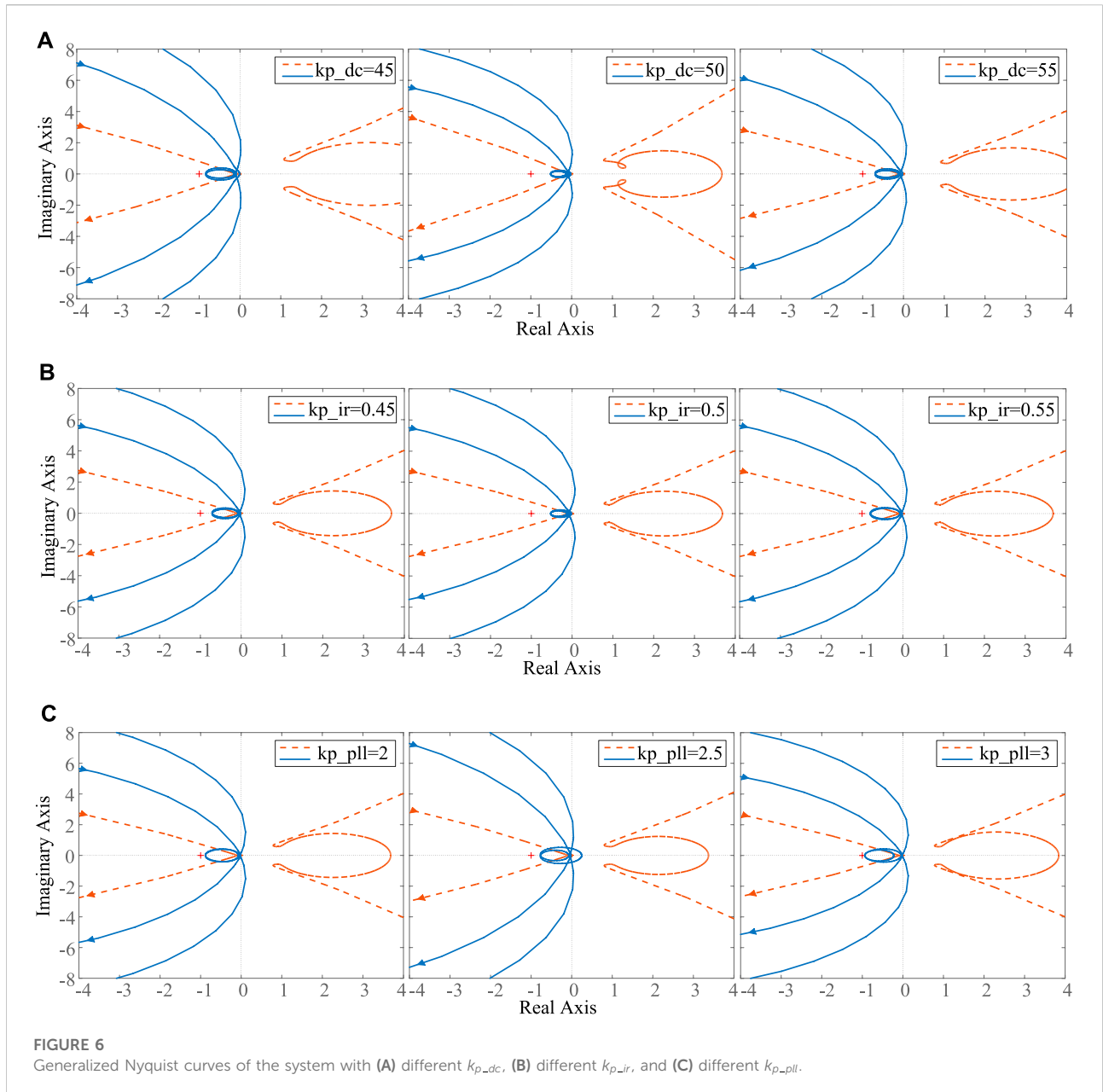Clustering evaluation indexes. **(A)** Profile coefficient; **(B)** Average profile coefficient; **(C)** CHI.

FIGURE 6
Generalized Nyquist curves of the system with **(A)** different k_{p_dc}, **(B)** different k_{p_ir}, and **(C)** different k_{p_pll}.

difference between adjusted R^2 and predicted R^2 is less than 0.2. From Table 8, it can be found that the statistics of the model all meet the requirements, indicating that the fit and correlation of the model are good and the error is small, so it can also predict OD under different combinations of operating parameters.

A quadratic multiple regression is fitted to a total of 51 data points from 17 sets of experiments to create a regression equation as in (24). The response surface of each factor combination on OD is depicted in Figure 7.

$$OD = 35.72 - 9.19A + 2.85B - 2.21C - 0.4965AB - 0.0402AC + 1.26BC - 0.1256A^2 + 12.16B^2 + 0.3401C^2$$

$$(24)$$

As shown in Figure 7A, OD decreases and then rises as k_{p_ir} increases from 0.45 to 0.55, and there is a minimal value between 0.47 and 0.51; when k_{p_ir} is small, OD decreases gradually with the increase of k_{p_dc} from 45 to 55, and the decrease in OD increases as k_{p_ir} increases. From Figure 7B, OD tends to decrease as k_{p_pll} increases from 2 to 3 and is flatter; OD decreases rapidly as k_{p_dc} increases. From Figure 7C, OD gradually decreases as k_{p_pll} increases, and the effect of k_{p_ir} on OD is much more significant than that of k_{p_pll}. As shown in Figure 7, the interaction between k_{p_ir} and k_{p_pll} is significant, which is consistent with the ANOVA results.

TABLE 7 ANOVA results for *OD* of RSM.

Source	Sum of squares	df	Mean square	F-value	P-value	Significance
Model	1415.17	9	157.24	217.94	<0.0001	***
A-k_{p_dc}	675.44	1	675.44	936.17	<0.0001	***
B-k_{p_ir}	64.81	1	64.81	89.83	<0.0001	***
C-k_{p_pll}	39.22	1	39.22	54.36	0.0002	**
AB	0.9861	1	0.9861	1.37	0.2806	—
AC	0.0065	1	0.0065	0.009	0.9272	—
BC	6.31	1	6.31	8.75	0.0212	*
A^2	0.0664	1	0.0664	0.092	0.7704	—
B^2	622.97	1	622.97	863.45	<0.0001	***
C^2	0.4871	1	0.4871	0.6751	0.4384	—
Residual	5.05	7	0.7215			—
Lack of fit	2.87	3	0.9555	1.75	0.2951	—
Pure error	2.18	4	0.546	—	—	—

P-value is the probability of significance. The smaller the *p*-value, the more significant the effect of the factor on the response value. $p < 0.0001$ indicates that the effect of the factor on the response value is extremely significant, denoted by ***; $p \leq 0.01$ indicates that the effect is highly significant, denoted by **; $0.01 < p \leq 0.05$ indicates that the effect is significant, denoted by *; $p > 0.05$ indicates that the effect is not significant.

TABLE 8 Statistics for *OD* of RSM.

C.V.%	R^2	Adjusted R^2	Predicted R^2	Adeq precision
2.04	0.9964	0.9919	0.9653	54.9497

The optimal solution that satisfies the optimization index can be obtained by optimizing *OD* through (24). The optimal predicted and experimental value can be calculated by substituting the corresponding factor values into the regression equation and simulation model and then the error between them can be obtained. The results are listed in Table 9.

Noticeably, the *OD* predicted by the model is 24.411, which is 1.33% lower than the minimum value of the response surface experiment (24.741). The error between the predicted and the experimental value is 2.3% (not more than 5%), indicating that the regression model is accurate and effective for the optimization.

4.4 Simulation results

To verify the effectiveness of the multi-parameter coupling optimization design strategy in this paper, the strategy combining the OEM and PSO in (Geng et al., 2019) is used for comparative verification. The SCR is changed from 3 to 2 and
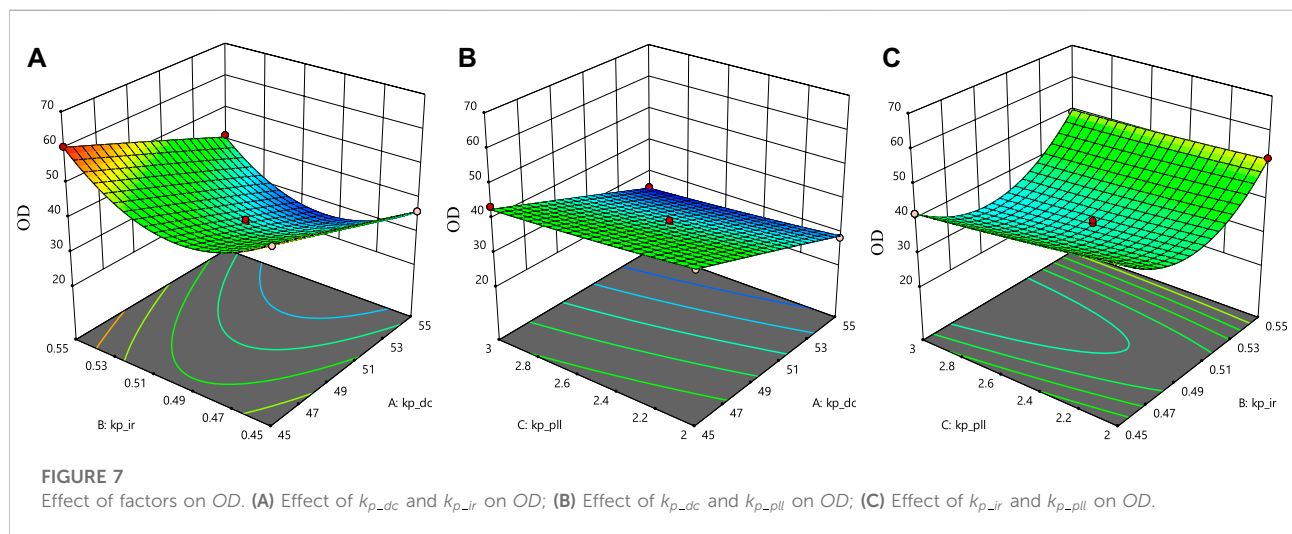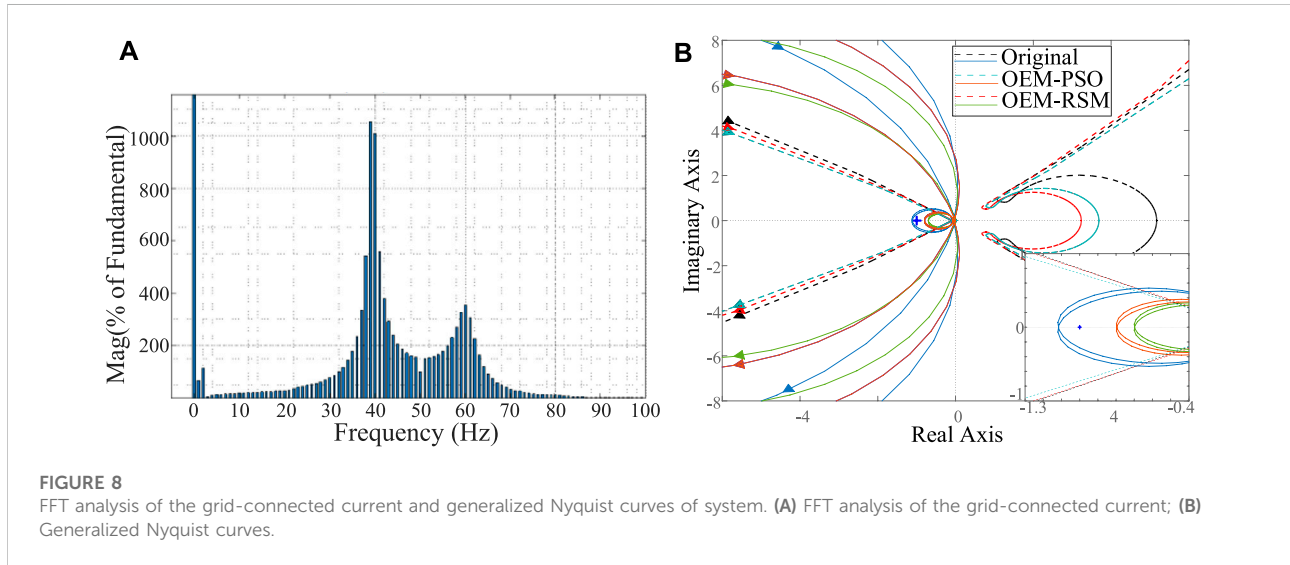

FIGURE 7
Effect of factors on *OD*. **(A)** Effect of k_{p_dc} and k_{p_ir} on *OD*; **(B)** Effect of k_{p_dc} and k_{p_pll} on *OD*; **(C)** Effect of k_{p_ir} and k_{p_pll} on *OD*.

TABLE 9 Optimal parameter combination based on RSM.

k_{p_dc}	k_{p_ir}	k_{p_pll}	Predicted	Experimental	Error (%)
54.961	0.495	2.979	24.411	24.986	2.3

Figure 10 illustrates the DC-link voltage, active power, and grid current angular frequency curves when the SCR is 3 and SCD is 20%, with a three-phase ground short-circuit fault occurring at 2 s and removed after 0.1 s. To facilitate the analysis, ΔU_{dc}, ΔP_s, and $\Delta \omega_s$ with 3 parameter combinations are calculated in Table 10.

FIGURE 8
FFT analysis of the grid-connected current and generalized Nyquist curves of system. (A) FFT analysis of the grid-connected current; (B) Generalized Nyquist curves.

SCD is changed from 20% to 60% at 2s. The FFT analysis of the grid-connected current and generalized Nyquist curves of the system after 2s are depicted in Figure 8. Figure 9 shows the d-axis stator current waveform.

The FFT analysis is used to determine the frequency at which oscillations occur in the grid-connected system. It can be found from Figure 8 that the system appears SSO with a frequency of 39 Hz (lower than power frequency 50 Hz). The generalized Nyquist curve after 2 s changes from enclosing (−1, j0) to not enclosing and gradually moving away when control parameters change from the original parameters to the optimized parameters, indicating that the system changes from unstable to stable. It can be observed from Figure 9 that the system is destabilized after the grid condition changes to very weak grid and high series compensation degree with the original parameters, resulting in divergent SSR. After optimization by the strategy proposed in this paper and the strategy in (Geng et al., 2019), the system oscillations converge. The d-axis stator current returns to stability after about 2 s with the optimized parameters of the OEM-PSO, whereas it only oscillates for about 0.7 s with the optimized parameters of the OEM-RSM. Apparently, both optimization methods are effective in improving the stability of the sub-synchronous state of the system, and the OEM-RSM is more effective. The simulation results are consistent with the theoretical analysis results.

FIGURE 9
D-axis stator current waveform.
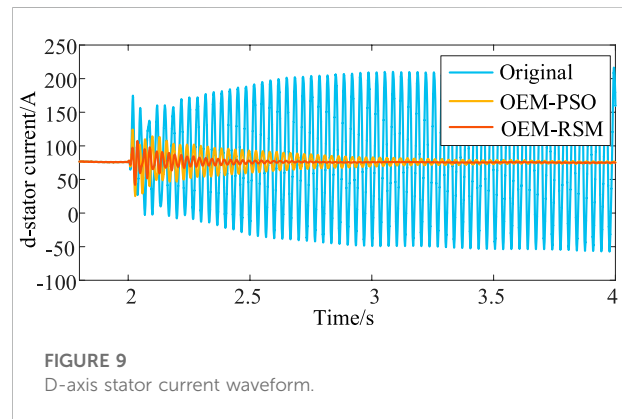
From Figure 10, after optimization of the proposed strategy, the overshoot and settling time of DC-link voltage, active power, and grid current angular frequency with disturbance are much smaller, and the fluctuation is significantly weakened and the anti-interference is strongly enhanced. It can be found from Table 10 that ΔU_{dc}, ΔP_s, and $\Delta \omega_s$ with the optimized parameters of the OEM-PSO and the OEM-RSM are both reduced. Visibly, ΔU_{dc} is reduced by 26.65%, ΔP_s is reduced by 12.83%, and $\Delta \omega_s$ is reduced by 46.70% compared to the original parameters after optimization by the OEM-RSM. In conclusion, both optimization methods can improve the dynamic
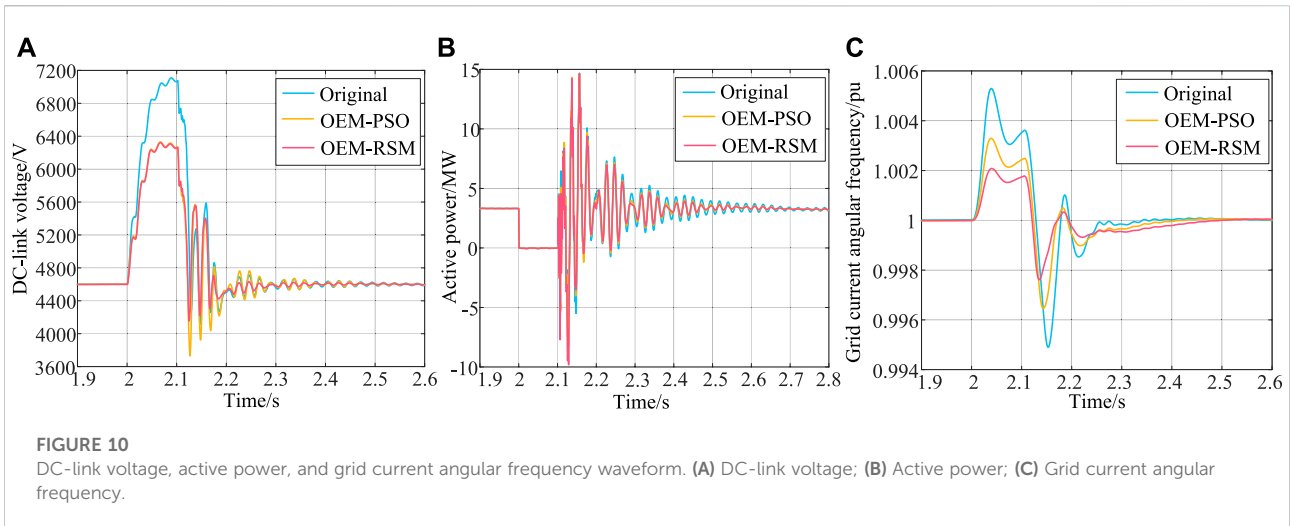
FIGURE 10
DC-link voltage, active power, and grid current angular frequency waveform. **(A)** DC-link voltage; **(B)** Active power; **(C)** Grid current angular frequency.

TABLE 10 Results of evaluation indexes with 3 parameter combinations.

Evaluation indexes	ΔU_{dc}/V	ΔP_s/MW	$\Delta \omega_s$/pu
Original	67.9229	1.1119	6.3085E-4
OEM-PSO	56.1519	1.0037	4.5033E-4
OEM-RSM	49.8196	0.9692	3.3627E-4

characteristics of the system. Moreover, the OEM-RSM is more effective in optimizing both the SSO characteristics and dynamic stability.

5 Conclusion

Based on the model of DFIG-based wind farm connected to weak grid by series compensation system, this paper proposes a clustering method based on the PCA and WFCM algorithm, with the dominant variables of the system SSO mode as the initial clustering indexes. For the equivalent wind farm after clustering, the DFIG control parameters are taken as the optimization object, and the sub-synchronous state stability and dynamic characteristics of the system are simultaneously optimized as the optimization objective. The optimal design strategy combining the OEM and RSM is adopted to quantitatively evaluate the interaction between controller parameters and the significance of their effects on the SSO and dynamic characteristics of the grid-connected system. The optimal parameter combination is obtained to achieve the effective mitigation of SSO. The highlights are as follows:

1) The proposed equivalence modeling method for DFIG-based wind farm takes into account the correlation between clustering indexes and SSO mode as well as the contribution degree of different clustering indexes to clustering results. It eliminates the redundancy of data and can be applied to study SSO in large-scale wind farm grid-connected systems.
2) Compared with the OEM-PSO, the proposed multi-parameter coupling optimization strategy can effectively improve the anti-interference and system stability in the sub-synchronous state, which can be applied to study the optimization problems of complex systems with multiple parameters and indexes.
3) k_{p_dc}, k_{p_ir}, and k_{p_pll} have significant effects on SSO characteristics and dynamic characteristics of the system, and there is a strong interaction between k_{p_ir} and k_{p_pll}.

In addition, the current work will also be carried out for better analyzing and solving the SSO problem in actual situations in the near future. Since the control parameters of each cluster are changed synchronously in this paper, the interaction between clusters and the influence of control parameters of different clusters at different locations on SSO characteristics of the system will be fully considered to improve the proposed strategy.

Data availability statement

The original contributions presented in the study are included in the article/Supplementary Material, further inquiries can be directed to the corresponding author.

Author contributions

Funding

Conflict of interest

The authors declare that the research was conducted in the absence of any commercial or financial relationships that could be construed as a potential conflict of interest.

Publisher's note

All claims expressed in this article are solely those of the authors and do not necessarily represent those of their affiliated organizations, or those of the publisher, the editors and the reviewers. Any product that may be evaluated in this article, or claim that may be made by its manufacturer, is not guaranteed or endorsed by the publisher.

References

Bakir, H., Merabet, A., Dhar, R. K., and Kulakistet, A. A. (2020). Bacteria foraging optimisation algorithm based optimal control for doubly-fed induction generator wind energy system. *IET Renew. Power Gener.* 14 (11), 1850–1859. doi:10.1049/iet-rpg.2020.0172

Chen, A., Xie, D., Zhang, D., Gu, C., and Wang, K. (2019). PI parameter tuning of converters for sub-synchronous interactions existing in grid-connected DFIG wind turbines. *IEEE Trans. Power Electron.* 34 (7), 6345–6355. doi:10.1109/tpel.2018.2875350

Chen, Y., Wu, H., and Shi, J. (2018). Application of singular value decomposition algorithm to dimension-reduced clustering analysis of daily load profiles. *Automation Electr. Power Syst.* 42 (3), 105. doi:10.7500/AEPS20170309008

Dong, X., Hou, J., Tian, X., and Liu, Y. (2016). Comparison of the impact level on subsynchronous resonance characteristics of dominant factors by multiple wind farms at different locations. *High. Volt. Eng.* 42 (07), 2259. doi:10.13336/j.1003-6520.hve.20160713029

Geng, J., Qian, X., and Zhou, S. (2019). New fuzzy clustering validity index. *Appl. Res. Comput.* 36 (4), 1001. doi:10.19734/j.issn.1001-3695.2017.10.0991

Han, J., Miao, S., Li, L., Yang, W., and Li, Y. (2020). Wind turbines clustering in wind farm based on multi-view transfer learning and synthetic optimization of parameters in equivalent wind farm. *Proc. CSEE* 40 (15), 4866. doi:10.13334/j.0258-8013.pcsee.190952

Han, K. L., Huang, T. W., and Yin, L. F. (2021). Quantum parallel multi-layer Monte Carlo optimization algorithm for controller parameters optimization of doubly-fed induction generator-based wind turbines. *Appl. Soft Comput.* 112, 107813. doi:10.1016/j.asoc.2021.107813

Hu, B., Nian, H., Li, M., Xu, Y., Liao, Y., and Yang, J. (2022). Impedance-based analysis and stability improvement of DFIG system within PLL bandwidth. *IEEE Trans. Ind. Electron.* 69 (6), 5803–5814. doi:10.1109/tie.2021.3088369

Huang, J., Wu, X., Zheng, Z., Huang, Y., and Li, W. (2022). Multi-objective optimal operation of combined cascade reservoir and hydrogen system. *IEEE Trans. Ind. Appl.* 58 (2), 2836–2847. doi:10.1109/tia.2021.3138949

Lei, H., Zhen, C., Yue, X., Xu, G., and Bao, J. (2013). Mitigating thermal power's SSR by additional damping controller of DFIG. *Electr. Power* 46 (4), 63. doi:10.3969/j.issn.1004-9649.2013.04.014

Leon, A. E., Amodeo, S. J., and Mauricio, J. M. (2021). Enhanced compensation filter to mitigate subsynchronous oscillations in series-compensated DFIG-based wind farms. *IEEE Trans. Power Deliv.* 36 (6), 3805–3814. doi:10.1109/tpwrd.2021.3049318

Li, C., Cai, W., Zhao, R., Yu, C., and Zhang, Q. (2019). Power consumption behavior analysis of AP cluster users based on optimized SAX and weighted load characteristic index. *Trans. China Electrotech. Soc.* 34 (S1), 368. doi:10.19595/j.cnki.1000-6753.tces.l80097

Liu, J., Yao, W., Wen, J., Fang, J., Jiang, L., He, H., et al. (2020). Impact of power grid strength and PLL parameters on stability of grid-connected DFIG wind farm. *IEEE Trans. Sustain. Energy* 11 (1), 545–557. doi:10.1109/tste.2019.2897596

Liu, J., Yao, W., and Wen, J. (2017). Small signal stability analysis and control of double-fed induction generator considering influence of PLL and power grid strength. *Proc. CSEE* 37 (11), 3162. doi:10.13334/j.0258-8013.pcsee.160857

Liu, M., Pan, W., Zhang, Y., Zhao, K., Zhang, S., and Liu, T. (2019). A dynamic equivalent model for DFIG-based wind farms. *IEEE Access* 7, 74931–74940. doi:10.1109/access.2019.2918359

Ma, X., Yang, Q., Chen, C., Luo, H., and Zheng, D. (2021). Harmonic and interharmonic analysis of mixed dense frequency signals. *IEEE Trans. Ind. Electron.* 68 (10), 10142–10153. doi:10.1109/tie.2020.3026288

Miao, Z. X. (2012). Impedance-model-based SSR analysis for type 3 wind generator and series-compensated network. *IEEE Trans. Energy Convers.* 27 (4), 984–991. doi:10.1109/tec.2012.2211019

Pan, X., Zhang, C., and Ju, P. (2015). Coherency-based dynamic equivalence of wind farm composed of doubly fed induction generators. *Power Syst. Technol.* 39 (03), 621. doi:10.13335/j.1000-3673.pst.2015.03.006

Shabanikia, N., Nia, A. A., Tabesh, A., and Khajehoddin, S. A. (2021). Weighted dynamic aggregation modeling of induction machine-based wind farms. *IEEE Trans. Sustain. Energy* 12 (3), 1604–1614. doi:10.1109/tste.2021.3057854

Si, J., Zhao, S., Feng, H., Cao, R., and Hu, Y. (2018). Multi-objective optimization of surface-mounted and interior permanent magnet synchronous motor based on taguchi method and response surface method. *Chin. J. Electr. Eng.* 4 (1), 67. doi:10.23919/CJEE.2018.8327373

Sun, Y., Mao, Y., Li, Z., Zhang, X., and Li, F. (2021). A comprehensive clustering method of user load characteristics and adjustable potential based on power big data. *Proc. CSEE* 41 (18), 6259. doi:10.13334/j.0258-8013.pcsee.201928

Wang, Z., Yang, C., Oh, S. -K., Fu, Z., and Pedrycz, W. (2020). Robust multi-linear fuzzy SVR designed with the aid of fuzzy C-means clustering based on insensitive data information. *IEEE Access* 8, 184997–185011. doi:10.1109/access.2020.3030083

Wanigasekara, C., Swain, A., Almakhles, D., and Zhou, L. (2022). Design of delta–sigma-based PID controller for networked wind energy conversion systems. *IEEE Trans. Ind. Appl.* 58 (1), 879–889. doi:10.1109/tia.2021.3126574

Xia, Y., Chen, Y., Song, Y., and Strunz, K. (2020). Multi-scale modeling and simulation of DFIG-based wind energy conversion system. *IEEE Trans. Energy Convers.* 35 (1), 560–572. doi:10.1109/tec.2019.2953893

Zhang, F., Yuan, H., Zhou, B., Zhang, Q., and Jin, X. (2022). "Parameter optimization and SSR mitigation of DFIG considering PLL," in 2022 Power System and Green Energy Conference (PSGEC), 430

Zhao, K., Dai, Y., Jia, Z., and Ji, Y. (2022). General fuzzy C-means clustering strategy: Using objective function to control fuzziness of clustering results. *IEEE Trans. Fuzzy Syst.* 30 (9), 3601–3616. doi:10.1109/tfuzz.2021.3119240

Zhou, Y., Zhao, L., Matsuo, I., and Lee, W. (2019). A dynamic weighted aggregation equivalent modeling approach for the DFIG wind farm considering the weibull distribution for fault analysis. *IEEE Trans. Ind. Appl.* 55 (6), 5514–5523. doi:10.1109/tia.2019.2929486